Construction and Building Materials 29 (2012) 458–465

Contents lists available at SciVerse ScienceDirect

Construction and Building Materials

journal homepage: www.elsevier.com/locate/conbuildmat

Review

Ground-penetrating radar for the structural evaluation of masonry bridges: Results and interpretational tools

M. Solla *, H. Lorenzo, F.I. Rial, A. Novo

Department of Natural Resources & Environmental Engineering, University of Vigo, A Xunqueira, 36005 Pontevedra, Spain

ARTICLE INFO

Article history:
Received 29 November 2010
Received in revised form 31 August 2011
Accepted 2 October 2011
Available online 29 November 2011

Keywords:
Non-destructive evaluation
GPR
FDTD modelling
Masonry structures

ABSTRACT

Ground-penetrating radar (GPR) has shown good potential in providing valuable information for the evaluation of masonry structures. We used GPR to survey several stone arch bridges located in the Galician territory in Spain. The results revealed previously unknown geometrical data and hidden characteristics of the interiors of the bridges, including the presence of internal voids, ancient arches, and restorations. However, many factors can adversely affect a GPR survey, such as ringing noise and signal attenuation. These factors can make data interpretation complex. To assist in the interpretation, we employed numerical modelling because it can play a very important role in extracting valid and useful information from GPR data sets. The expected electromagnetic wave response can be simulated through the use of modelling tools. The obtained information can be useful for engineers, as it provides better structural knowledge of the bridge.

Contents

1. Introduction

Ancient stone masonry arch bridges are still commonly in use within the transport infrastructure. Many of these structures require special attention and monitoring. Increases in traffic load and intense vibrations since they were designed can result in structural decay [1,2]. Therefore, ongoing diagnosis of their changing structural integrity is required to provide information to help with their preservation and restoration.

In the last several decades, there has been a continuous increase in the use of non-destructive testing (NDT) to evaluate civil engineering structures [3,4]. Ground-penetrating radar (GPR) is an NDT method that is used for evaluating masonry bridges [5]. Nevertheless, there have been are few published studies on testing stone masonry bridges using GPR, with some notable exceptions [6–12]. These studies have provided promising information about the hidden geometry, bridge foundations, ring stone thickness, moist zones, and fill conditions in masonry bridges.

There are many stone arch bridges in the Autonomous Community of Galicia (northwest Spain) [13]. For this work, we studied 36 stone masonry arch bridges located in the Galician territory (Fig. 1). Our objectives were to analyse the viability and effectiveness of GPR in obtaining previously unknown, inner details for the assessment of these structures. The knowledge of this structural information is important for civil engineers engaged in developing future conservation and strengthening techniques.

Many factors can adversely affect GPR waves, including ringing noise, airwave events, and signal attenuation. Data interpretation can become complex because of these unfavourable events. Therefore, several factors should be taken into account to improve the interpretation of the GPR data. These factors include the establishment of survey objectives, compilation of all available structural and geometrical information about the bridge, and knowledge of

* Corresponding author. Tel.: +34 986 801908; fax: +34 986 801907.
E-mail address: merchisolla@uvigo.es (M. Solla).

0950-0618/$ - see front matter © 2011 Elsevier Ltd. All rights reserved.
doi:10.1016/j.conbuildmat.2011.10.001

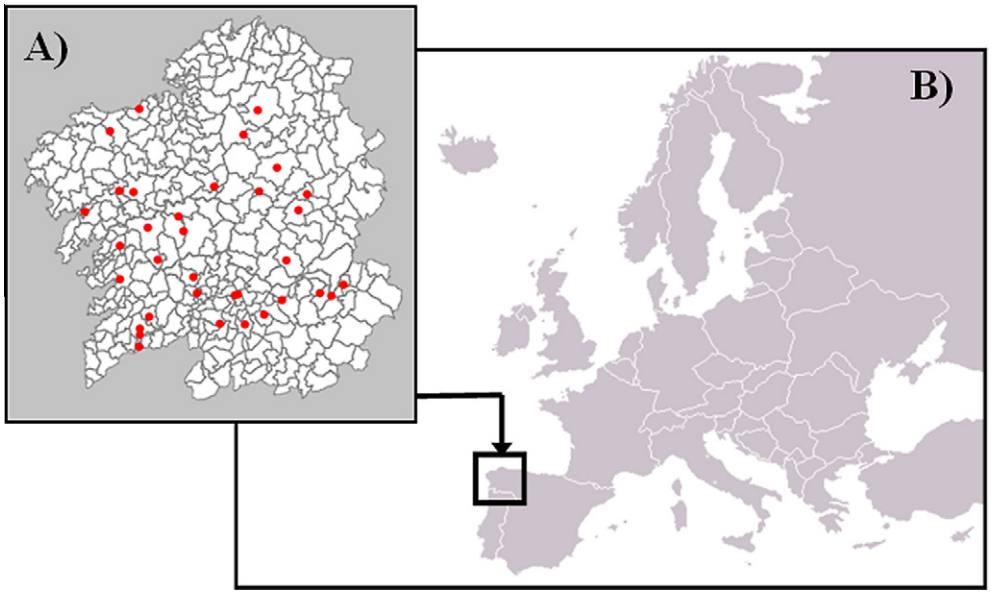

Fig. 1. (A) Stone masonry bridges surveyed from the Galician territory and (B) location of Galicia (northwest Spain) in Europe.

the building materials used and possible bridge restorations performed. For example, knowledge of the arch span (Fig. 2) would help to establish an estimate of the different radar wave velocities in the stonework. Using this structural information, we estimated the radar wave velocity for solid ashlars by adapting diffraction hyperbolas [14] to the hyperbolic reflection produced by the arch–air interface.

The analysis and interpretation of GPR data from heterogeneous stone masonry structures can be complicated. To assist in the interpretation, we employed numerical modelling. Processed GPR data can be compared to models to aid in the interpretation of data from complex environments [15]. Many numerical modelling methods are available for simulating the propagation of GPR waves in different media [16]. The finite-difference time domain (FDTD) technique [17,18] has evolved into one of the most popular advanced modelling tools [16] and is used when a more sophisticated interpretation is required. This modelling method allows for the extraction of subtle information from the real data, such as diffraction events and the presence of reflection multiples [19]. However, few studies using both FDTD modelling and field GPR data to evaluate masonry arch bridges have been published to date [20,21].

2. Methodology

We collected our data with a RAMAC GPR system, manufactured by MALÅ Geoscience, using shielded antennas with centre frequencies of 250 and 500 MHz. We chose these two centre frequencies in order to achieve both resolution and penetration for analysing the fill material and, the bridge foundations. For all of the bridges we studied, we collected two parallel longitudinal profiles, in opposite directions along the bridge, with each antenna (Fig. 3). We acquired the data using the common–offset mode with the antenna polarisation perpendicular to the data collection direction. The distance between the profiles was set to 1 m, as shown in Fig. 3. In most cases, for the 250 MHz data, the in-line spacing and the total time window were equal to 5 cm and 200 ns, respectively, and were defined by 516 samples per trace. For the 500 MHz data, the in-line spacing was equal to 2 cm, and the total time window was set to 100 ns, which was also defined by 678 samples per trace. We used an odometer wheel attached to the antenna to measure the profile lengths. However, some of the bridges had intact ancient flagstone surfaces composed of large irregular blocks (Fig. 3), which made measurements difficult as the continuous movement of the survey wheel was interrupted. Therefore, we calibrated the wheel on-site to avoid inaccuracies in spatial trace positioning.

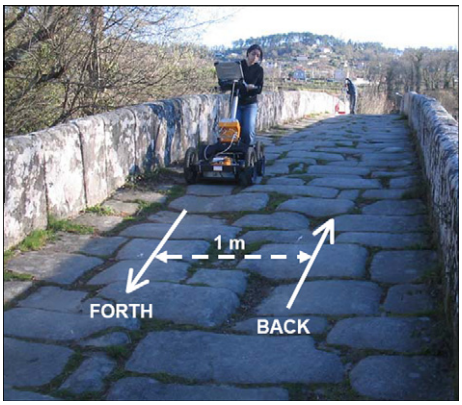

Fig. 3. GPR survey, using the 500 MHz antenna, composed of two parallel profiles through the Cernadela Bridge in opposite directions.

We processed our data with ReflexW v.5.6 software, and we applied the following processing sequence: time-zero correction, dewow filtering, gain application (*Gain function* (with linear and exponential part [14])), and spatial (*Subtracting average*). In some cases, a band-pass (*Butterworth*) filter was also applied. The objective

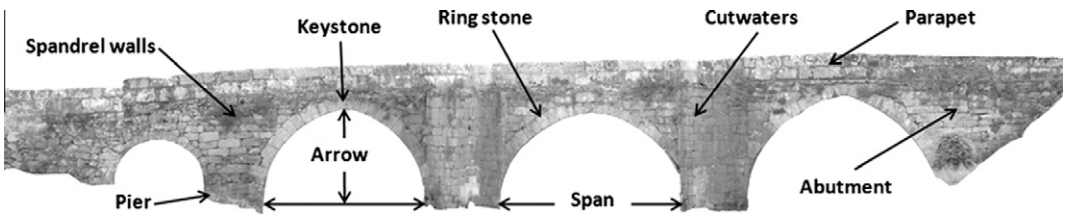

Fig. 2. Two-dimensional orthophotograph of the Traba Bridge showing the components and definitions used in masonry arch bridges.

Table 1
Data processing (ReflexW v.5.6 software) applied to the GPR data acquired with the 250 and 500 MHz shielded antennas.

250 MHz		500 MHz	
Step	Details	Step	Details
1	Time-zero correction	1	Time-zero correction
2	Dewow filtering	2	Dewow filtering
3	Gain function (linear 1.0 and exponential 0.5)	3	Gain function (linear 1.0 and exponential 0.4)
4	Subtracting average (150 average traces)	4	Subtracting average (200 average traces)
5	Band-pass Butterworth (low cutoff 100 MHz; upper cutoff 350 MHz)	5	Band-pass Butterworth (low cutoff 300 MHz; upper cutoff 900 MHz)
6	Topography correction based on velocity = 0.11 m/ns	6	Topography correction based on velocity = 0.11 m/ns

was to correct the down-shifting of the radar section due to the air–ground interface and to amplify the received signal, as well as to remove both low and high-frequency noise in the vertical and horizontal directions. In addition, we applied corrections for topography and the tilt of the antenna when the bridge had an upward arching profile to improve the accuracy in imaging subsurface features [22]. In those cases, we performed topographic surveys to obtain elevation variations of the GPR profiles. Without static corrections, the location of subsurface features can change, and the shape of features becomes distorted. Table 1 shows the processing sequences applied and the parameters most commonly used for the filters.

For some bridges, a three-dimensional model of the whole bridge was constructed using photogrammetric or laser scanning methods. As a result of this process, we created two-dimensional orthophotographs of the structure at the locations where the main geometrical parameters were measured. The metric information obtained allowed us to calculate accurate radar wave velocities for granitic masonry in different zones of the structure. Knowledge of the most appropriate radar wave velocity allows for a more exhaustive interpretation of the GPR data. The velocity was estimated by adapting a diffraction hyperbola [14] to the hyperbolic reflection produced by the arch–air interface. We used the arch span geometry obtained to define the hyperbolic shape to fit. Nevertheless, the reflections generated from the arch–air interface can present an asymmetric shape on each side of the keystone (Fig. 2). This irregularity can be caused by many factors, such as the presence of different fills on both sides over the arch, in addition to irregular arch geometries such as segmental or gothic pointed arches. Next, some difficulties can occur in fitting a model of a hyperbolic shape to the reflection pattern generated. In such circumstances, we calculated the average velocity by adapting a hyperbolic shape to each half of the reflection, resulting in two different signal velocities.

Moreover, the precise geometry provided was used to elaborate on the FDTD modelling. Our purpose was to design a realistic, large-scale, synthetic GPR model of the entire bridge to assist in the interpretation of the processed field data. However, simulating large-scale and realistic models requires high performance computing to obtain a result in a reasonable amount of time. The need to discretise the volume of the problem space and the staircase approximation of curved interfaces to the real boundary result in excessive computer memory requirements and large execution times. We created our synthetic models using a parallelised version – based on MPI and Open MP – of GprMax [23], which is an electromagnetic wave simulator for GPR using the FDTD method. Using a mixed model of parallelisation, where different traces are computed at different nodes of a cluster, we obtained a significant reduction in computational time. The FDTD algorithm was previously developed using the MATLAB environment.

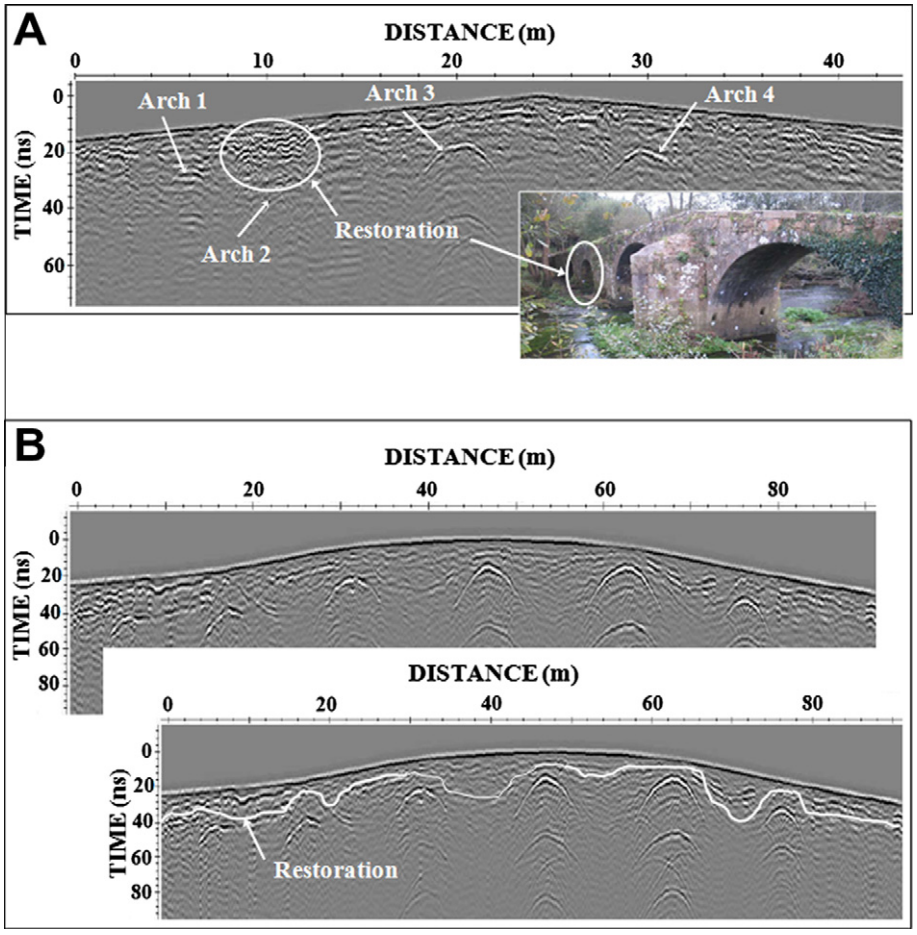

Fig. 4. GPR results. (A) Processed radargram acquired with the 500 MHz antenna in the Lubians Bridge, showing the effect of a restoration performed over the second arch and (B) processed data obtained in the Monforte Bridge using the 250 MHz, which illustrates the reflection produced by a pathway restoration.

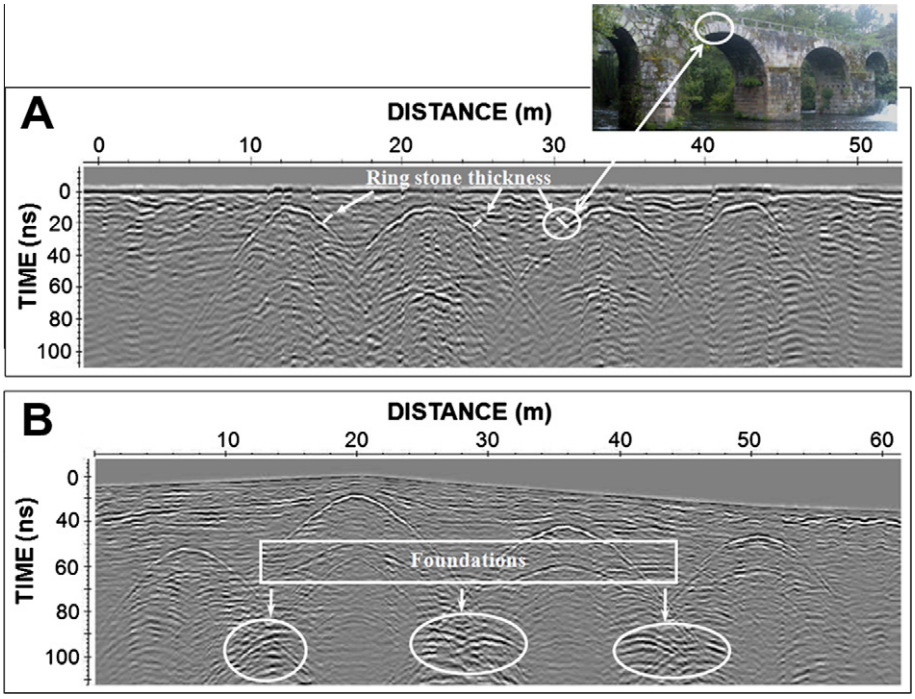

Fig. 5. GPR results acquired with the 250 MHz antenna. (A) Processed radargram obtained from the O Freixo Bridge, which reveals the ring stone thickness and (B) processed data collected at the Areas Bridge, where the bridge foundations are interpreted to be on bedrock because of the strong signal at the pier-bedrock interface.

3. Results and discussion

We obtained results that provided information from historical, archaeological and civil-structural points of view. By observing the anomalies in the reflection patterns, it was possible to detect and map the remains of previously performed restorations of the bridges, such as the reconstruction of arches (Fig. 4A) and the pathways of some bridges (Fig. 4B). In the case of the restored arch (Fig. 4A), we can observe a different reflection pattern generated just above this arch. This difference in reflection occurs when sufficient contrast, in terms of homogeneity, exists between the original fill materials and those used for the restoration. On the other hand, a pathway restoration can be identified from the reflection generated at the interface between the original and new fill materials (Fig. 4B), where the bridge structure may have been emptied and later refilled with different fill materials than the original ones. This reflection is a consequence of the high dielectric contrast between the fill materials. Additionally, differences in building materials in the same stonework were identified in some bridges. As in the case of the Lugo Bridge, the existence of slate fill would probably be detected by the attenuation of the radar wave in comparison with granitic fill [21].

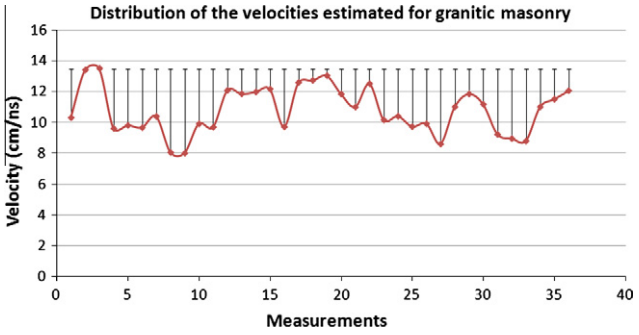

Fig. 6. Distribution of the calculated radar wave velocities for granitic masonry. These values were determined from all the bridges studied. The differences between the published average velocity in dry granitic masonry (13.5 cm/ns) and the calculated velocities are also illustrated.

From an archaeological point of view, it was possible to identify other interesting aspects, such as the presence of possible hidden arches [12] or a different historical shape of the structure [21]. In the case of a hidden arch, the signal response is a hyperbolic reflection (the same identified at the arch–air interface of visible arches), and the polarity of the signal can show whether the arch is empty or filled. A shift in the polarity, in relation to the signal at the arch–air interface, could result because the arch is filled (an extended explanation can be found in [12]). In some medieval bridges, the former double slope profile had been filled to create a horizontal pathway using a different fill material, which presents dielectric properties with sufficient contrast, with respect to the original material, to distinguish in the data. In these cases, we observed a slightly sloping constant reflector at both margins of the bridge structure [21].

Structural information was also interpreted. Solid piers for bridge reinforcement were identified as a constant reflection at the interface between the masonry and solid granite [12]. The detection of variations in the inner materials was made possible by their high dielectric contrasts. Rarely, we identified the ring stone thickness (Fig. 5A), where a hyperbolic reflection is produced by the fill-stone interface. This reflection is very similar to that obtained at the solid stone–air interface. The main difference is the expected consequent shift in the signal polarity produced at the fill-stone interface. Nevertheless, in most cases, the fill-stone interface is characterised by a fine signal due to the smaller dielectric contrast between the media. We sometimes obtained information about the nature of the bridge foundations. For example, when the pier of the bridge is lies on bedrock, the reflection at the interface showed a rather strong signal due to the large dielectric contrast between the materials (Fig. 5B). However, when the pier was in a sand river-bed, the reflections at the interface were not identified.

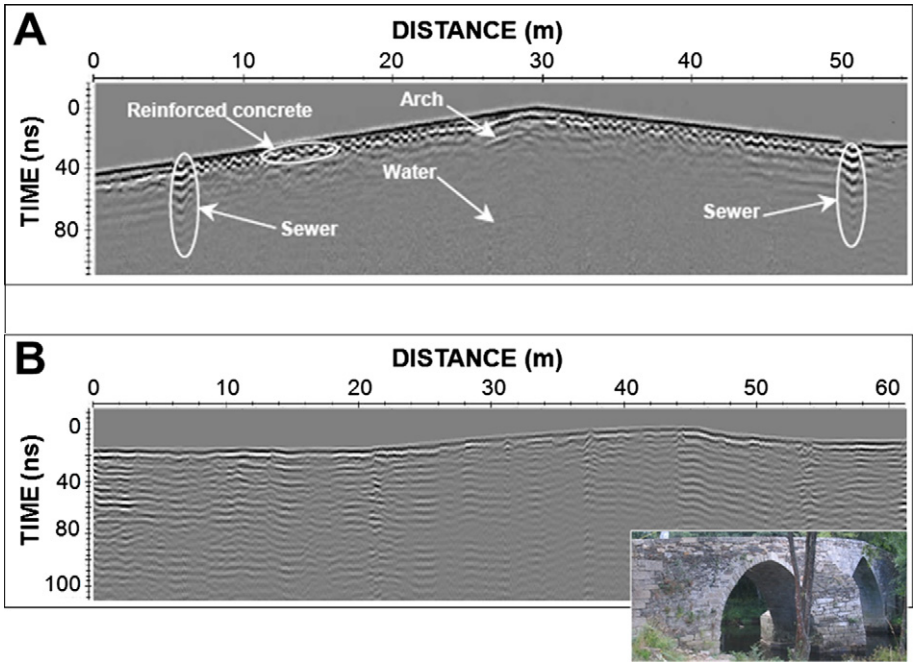

Fig. 7. GPR results acquired with the 250 MHz antenna. (A) Processed data collected at the Loña Bridge, showing the effect of the reinforced concrete and (B) processed results gathered at the San Alberte Bridge, where no reflections were identified (the severe signal attenuation was probably produced by the presence of soil–cement in the pathway).

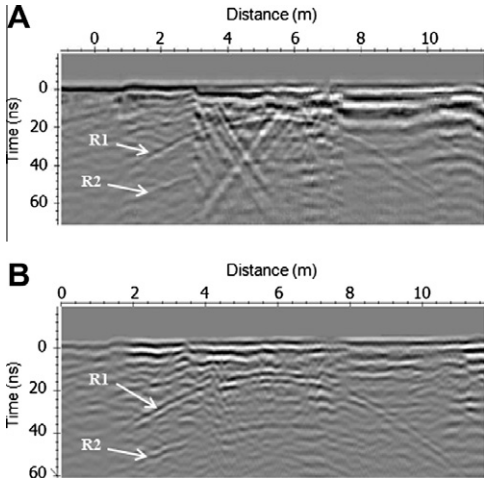

Fig. 8. (A) 250 MHz data from the Sarela Bridge showing the "*X Marks the spot*" in addition to the arch–air (R1) and air–water (R2) interfaces, and (B) GPR data after applying the "*Butterworth*" band-pass filter (150/350 MHz).

Moreover, a probable cavity was detected in one pier of the Traba Bridge [24], and the associated anomaly was a strong signal (with greater amplitude) from the high dielectric contrast between the masonry and the water.

The average velocity for granitic masonry was calculated in different zones of the structures. We estimated these velocity values using the external geometry of the bridge. The procedure for the calculations was explained in a previous section, and an average velocity was determined for each bridge. Fig. 6 shows the distribution of all of the estimated radar wave velocities, which ranged from 8.0 to 13.5 cm/ns. The typical average velocity in dry granitic masonry is reported in the literature as approximately 13.5 cm/ns [8,25]. However, the velocities in some of our case studies were much lower. The differences between the published and calculated values are illustrated in Fig. 6, where the average difference was 2.7 cm/ns. These velocity differences may be a consequence of inhomogeneities in the masonry (such as differences in composition and density), in addition to the probable presence of moist zones in the stonework. Other authors have also reported lower values of 10.5–11.5 cm/ns in wet granitic masonry [8]. In this work, the identification of cracks and voids within the bridge structure was not possible using GPR because of the confluence of the reflections from the non-homogeneous fill material. However, the existence of moist areas can be related to faults existing in the stonework.

We obtained additional structural information from the GPR data, including the identification of modern materials, such as reinforced concrete (Fig. 7A), which is frequently used in pathway construction for reinforcing the bridge subsurface. A reflection pattern was differentiated in the form of consecutive small hyperbolas. The same reflection pattern was also observed in other cases [24]. These new materials used for restoration could be an important cause of signal attenuation and loss of target resolution. As an example, Fig. 7B shows the GPR data acquired with a 250 MHz antenna in the restored San Alberte Bridge. Although this bridge has two large arches (see photograph in Fig. 7B), any hyperbolic reflections from the arch–air and air–water interfaces were identified in the radargram. This severe signal attenuation was most probably caused by the presence of a soil–cement mix used for sub-grade reinforcement and protection. All of this information can be useful for civil engineers in developing future strengthening measures.

Other factors that can adversely affect a GPR survey, and consequently data interpretation, include ringing events that are likely caused when GPR signals interact with a metal object, such as sewers pipes buried in the bridge (see Fig. 7A), creating repeated reflections within the object, and airwave events associated with leaking waves above the air–bridge interface. Part of this leaking energy reflects back and is recorded by the GPR receiver. Fig. 8A shows the 250 MHz data recorded in the Sarela Bridge, where the rare "*X Marks the spot*" could be identified. This effect most

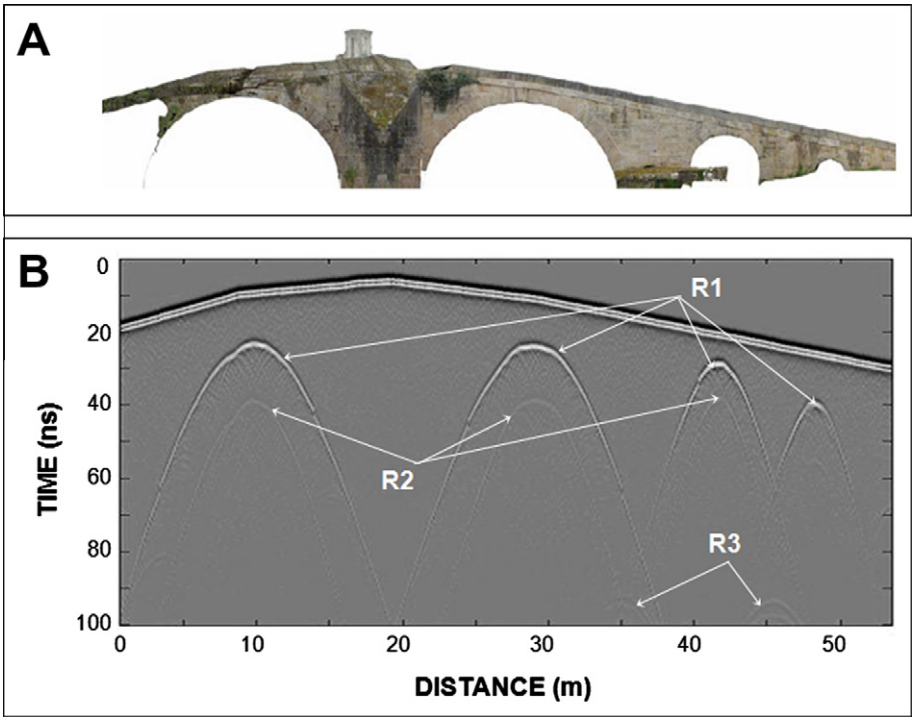

Fig. 9. The Carracedo Bridge. (A) Two-dimensional orthophotograph of the bridge (from the upstream side) generated from the laser scanning data, and (B) synthetic profile of the whole structure based on the orthophotograph, where the reflection of the stone–air interface (R1), reflection multiples produced from the arch (R2), and reflections caused by the proximity between the arches (R3) were identified.

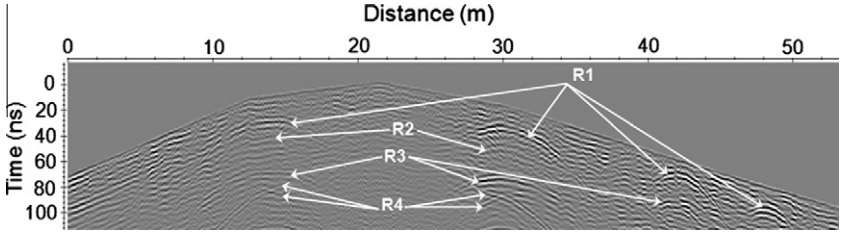

Fig. 10. Processed 250 MHz data from the Carracedo Bridge showing the interpretation of the main reflections identified, including those at the stone–air and air–water interfaces (R1, R3), reflection multiples from the arch (R2), and corner reflections (R4).

frequently appears when the GPR system is placed closed to a long wire, such as fence or cable, because the energy couples from the transmitter onto the wire [26]. The hyperbolic reflections from the arch–air (R1) and air–water (R2) interfaces are also observed in Fig. 8A. However, the reflection pattern generated by this event can make the identification of important smaller reflections difficult. Fortunately, we were able to remove all of the unwanted GPR signatures by applying appropriate signal processing techniques. In the particular case of the Sarela Bridge, the "*X Marks the spot*" was mostly removed after applying a "*Butterworth*" temporal band-pass filter (Fig. 8B). We defined this filter by setting the low-cut and high-cut frequencies to 150 and 350 MHz, respectively.

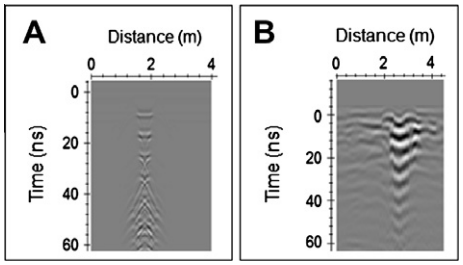

Fig. 11. Ringing noise caused by the reverberation of the GPR wave in a metal sewer. Comparison between synthetic (A) and field (B) 250 MHz data.

We developed synthetic models by considering the external geometry of the bridge and the orthophotograph produced by the photogrammetric or laser scanning data. We used these synthetic models to extract subtle information and to assist in the interpretation of the field GPR data. An example is presented in Fig. 9, which shows an FDTD synthetic radargram of the Carracedo Bridge generated by the corresponding orthophotograph. The model was created with a small spatial-step equal to 5 mm, and the excitation pulse was a Gaussian of 250 MHz centre frequency. The trace step and the total time window were 0.12 m and 100 ns, respectively. The relative permittivity assumed for the fill ranged from 4.0 to 9.0. Our purpose was to simulate a heterogeneous medium. We calculated these values using the GPR wave velocities provided by the field data. These values are similar to those proposed in the literature [25–27]. An FDTD algorithm was also developed, using the MATLAB environment, to correct our synthetic data for topography. Observing the synthetic results in

Fig. 9B, we identified the presence of reflection multiples produced from the arch (Fig. 9B:R2) and because of the proximity between arches (Fig. 9B:R3). These reflection multiples were also observed in the field GPR data (Fig. 10:R2). Moreover, the real data showed more complex reflections, such as those from the heterogeneous fill material between the arches and the corner reflections (Fig. 10:R4) from the perpendicular interfaces between the top of the vault and the water level [28]. Sometimes, more detailed FDTD models were needed to verify the interpretation of the field data; an example is the case of the Loña Bridge (Fig. 7A), where and additional model was used to analyse the ringing noise produced by the presence of a metal sewer pipe. We built a synthetic model by assuming a spatial-step of 16 mm and a 250 MHz centre frequency antenna. The trace step and the total time window were 0.01 m and 80 ns, respectively. The relative permittivity considered for the sewer pipe was 30.0. Fig. 11 shows both the synthetic (A) and field data (B), where the consequent ringing noise produced by the reverberation of the radar wave showed similar reflection patterns. All of these complex reflections, if unrecognised, can hinder the detection of other interesting reflectors.

4. Conclusions

A survey methodology to evaluate stone masonry bridges is presented in this work. We surveyed several masonry arch bridges using GPR with 250 and 500 MHz antennas. The field data were acquired using the common–offset mode with the antenna polarisation perpendicular to the data collection direction. The proposed methodology has the ability to provide information about internal bridge details. Valuable previously unknown information, such as hidden structural details, the geometry of ancient profiles, the existence of voids, and evidence of restoration and reconstruction tasks, was revealed. Nevertheless, we did not obtain clear information about the presence of cracks or moisture within the bridges.

The interpretation of the GPR data was sometimes complicated. Some modern materials used for restoration, such as reinforced concrete and soil–cement, as well as ringing noise and airwave events, can be additional causes of GPR signal attenuation and loss of target resolution. Appropriate data processing was therefore necessary to create accurate bridge images that allowed significant information to be extracted. The quality of our field data was improved using the signal processing applied here in. The GPR signal attenuation was corrected using a gain filter, which consists of amplifying the received signal. Both low and high frequency noise in the raw data was removed by temporal and spatial filtering. In some cases, processing was an essential tool for noise reduction and improved data interpretation. For example, in the Sarela Bridge, a "*Butterworth*" temporal band-pass filter was required to remove the rare "*X marks the spot*". The identification of other interesting reflections was difficult without this correction. It is important to note that appropriate signal processing should be carefully chosen and applied in a way that the data are not extremely distorted and spurious features are not introduced. Additionally, static corrections were considered in pointed arches to improve the accuracy of imaging subsurface features. Knowledge of the precise structural dimensions allowed the estimation of more appropriate radar wave velocities in masonry. The changes in velocity observed here potentially delineate the presence of different fills or moist areas in the stonework.

In addition, realistic FDTD models could provide subtle information that could help with data interpretation. The two-dimensional orthophotographs generated by laser scanning or photogrammetric data allowed the simulation of more realistic modelling scenarios using a mixed model of parallelisation. This approach encompasses the overall bridge structure in fine detail in a reasonable amount of time. In complex structures such as masonry bridges, it can be difficult to obtain an accurate interpretation without a comparison of the field data with the models.

One interesting future project would be the combination of GPR with other NDT techniques, such as infrared thermography, sonic and conductivity methods. Each NDT method provides different information regarding the physical properties of the masonry structure. This complementary testing could be useful in identifying cracks or voids in structures, changes in internal moisture, inhomogeneous areas and layering within the bridge. This additional information, if compared with GPR data, could assist in the interpretation.

Acknowledgments

The authors wish to acknowledge the financial support of the Spanish Ministry of Science and Innovation (Grant No. BIA2009-08012) and the facilities made available by the HPC-EUROPA2 project (Project Number: 228398) with the support of the European Commission – Capacities Area – Research Infrastructures. The useful suggestions supplied by Dr. Antonios Giannopoulos are also gratefully acknowledged.

References

[1] Forde MC. Bridge research in Europe. Constr Build Mater 1998;12(2–3):85–91.
[2] Bhandari NM, Kumar P. Structural health monitoring and assessment of masonry arch bridges. Adv Bridge Eng 2006:115–32.
[3] Popovics JS. NDE techniques for concrete and masonry structures. Prog Struct Eng Mater 2003;5:49–59.
[4] Leucci G, Cataldo R, Nunzio G. Assessment of fractures in some columns inside the crypt of the Cattedrale di Otranto using integrated geophysical methods. J Archaeol Sci 2007;34(2):222–32.
[5] McCann DM, Forde MC. Review of NDT methods in the assessment of concrete and masonry structures. NDT&E Int 2001;34:71–84.
[6] Colla C, Das PC, McCann D, Forde M. Sonic, electromagnetic and impulse radar investigation of stone masonry bridges. NDT&E Int 1997;30(4):249–54.
[7] Flint RC, Jackson PD, McCann DM. Geophysical imaging inside masonry structures. NDT&E Int 1999;32:469–79.
[8] Pérez-Gracia V. Radar de Subsuelo. Evaluación para Aplicaciones en Arqueología y en Patrimonio Histórico-Artístico. PhD thesis. Universidad Politécnica de Cataluña; 2001.
[9] Fernandes F. Evaluation of two novel NDT techniques: microdrilling of clay bricks and ground penetrating radar in masonry. PhD thesis. Universidade do Minho; 2006.
[10] Arias P, Armesto J, Di-Capua D, González-Drigo R, Lorenzo H, Pérez-Gracia V. Digital photogrammetry, GPR and computational analysis of structural damages in a medieval bridge. Eng Fail Anal 2007;14:1444–57.
[11] Lubowiecka I, Armesto J, Arias P, Lorenzo H. Historic bridge modelling using laser scanning, ground penetrating radar and finite element methods in the context of structural dynamics. Eng Struct 2009;31(11):2667–76.
[12] Solla M, Lorenzo H, Novo A, Rial FI. Ground-penetrating radar assessment of the medieval arch bridge of San Antón, Galicia, Spain. Archaeol Prospect 2010;17(4):223–32.
[13] Alvarado S, Durán M, Nárdiz C. Puentes históricos de Galicia. Colegio Oficial de Ingenieros de Caminos, Canales y Puertos. Xunta de Galicia; 1989.
[14] Sandmeier KJ. ReflexW manual v.4.5. From <http://www.sandmeier-geo.de>. Sandmeier Scientific Software. 435 pp. 2007.
[15] Millard SG, Shaw MR, Giannopoulos A, Soutsos MN. Modeling of subsurface pulsed radar for nondestructive testing of structures. ASCE J Mater Civil Eng 1998;10:188–96.
[16] Jol HM. Ground penetrating radar: theory and applications. Amsterdam: Elsevier Science; 2009. p. 524.
[17] Taflove A. Computational electrodynamics: the finite-difference time-domain method. London: Artech House; 1995.
[18] Yee KS. Numerical solution of initial boundary value problems involving Maxwells equations in isotropic media. IEEE Trans Anten Propag 1966;14(3):302–7.
[19] Giannopoulos A. Modelling ground penetrating radar by GprMax. Constr Build Mater 2005;19:755–62.
[20] Diamanti N, Giannopoulos A, Forde M. Numerical modelling and experimental verification of GPR to investigate ring separation in brick masonry arch bridges. NDT&E Int 2008;41(5):354–63.
[21] Solla M, Lorenzo H, Rial FI, Novo A. GPR evaluation of the Roman masonry arch bridge of Lugo (Spain). NDT&E Int 2011;44(1):8–12.
[22] Goodman D, Nishimura Y, Hongo H, Higashi N. Correcting for topography and the tilt of ground-penetrating radar antennae. Archaeol Prospect 2006;13(2):157–61.

[23] Giannopoulos A. GprMax2D/3D: electromagnetic simulator for ground probing radar; 2006. <http://www.gprmax.org>.
[24] Solla M, Lorenzo H, Riveiro B, Rial FI. Non-destructive methodologies in the assessment of the masonry arch bridge of Traba, Spain. Eng Fail Anal 2011;18(3):828–35.
[25] David J, Annan P. Ground-penetrating radar for high-resolution mapping of soil and rock stratigraphy. Geophys Prospect 1989;37:531–51.
[26] Annan P. GPR principles, procedures and applications. Sensors and Software, Inc.; 2003.
[27] Daniels DJ. Ground penetrating radar. London: The institution of Electrical Engineers; 2004.
[28] Martinaud M, Frappa M, Chapoulie R. GPR signal for the understanding of the shape and filling of man-made underground masonry. In: Proceedings of 10th international conference on ground penetrating radar; 2004.